Article

Cell Reports

Mitochondrial H_2O_2 in Lung Antigen-Presenting Cells Blocks NF-κB Activation to Prevent Unwarranted Immune Activation

Graphical Abstract

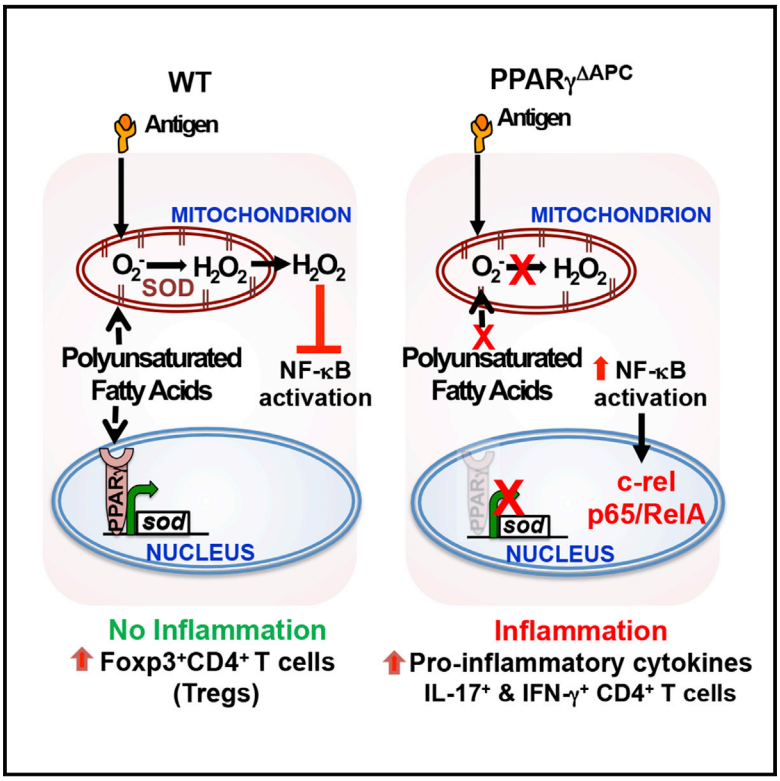

Highlights

- Immune tolerance invokes PPARγ-dependent mitochondrial H_2O_2 in lung immune cells
- PPARγ promotes superoxidase dismutase expression, which is central to H_2O_2 generation
- PPARγ-dependent mitochondrial H_2O_2 inhibits NF-κB activation to suppress inflammation
- PPARγ links the nucleus, mitochondria, and cell cytoplasm to ensure immune quiescence

Authors

Anupriya Khare, Mahesh Raundhal, Krishnendu Chakraborty, ..., Prabir Ray, Sruti Shiva, Anuradha Ray

Correspondence

raya@pitt.edu

In Brief

Khare et al. describe an essential role of PPARγ in maintenance of immune tolerance. Tolerance induction by inhaled antigen promotes PPARγ-dependent H_2O_2 generation in lung dendritic cells and macrophages involving mitochondrial metabolism requiring complex I activity. H_2O_2 suppresses NF-κB activation to prevent inflammatory T cell responses but supports Treg generation.

Khare et al., 2016, Cell Reports *15*, 1700–1714
May 24, 2016
http://dx.doi.org/10.1016/j.celrep.2016.04.060

CellPress

OPEN ACCESS
CellPress

Cell Reports
Article

Mitochondrial H_2O_2 in Lung Antigen-Presenting Cells Blocks NF-κB Activation to Prevent Unwarranted Immune Activation

Anupriya Khare,[1,8] Mahesh Raundhal,[1,8] Krishnendu Chakraborty,[1,8] Sudipta Das,[1] Catherine Corey,[2] Christelle K. Kamga,[2] Kelly Quesnelle,[3] Claudette St. Croix,[4] Simon C. Watkins,[4] Christina Morse,[1] Timothy B. Oriss,[1] Rachael Huff,[1] Rachel Hannum,[1] Prabir Ray,[1,5] Sruti Shiva,[2,6,7] and Anuradha Ray[1,5,*]

[1]Division of Pulmonary, Allergy and Critical Care Medicine, Department of Medicine
[2]Department of Pharmacology and Chemical Biology
[3]Department of Biomedical Sciences
Western Michigan University Homer Stryker School of Medicine, Kalamazoo, MI 49008, USA
[4]Department of Cell Biology
[5]Department of Immunology
[6]Vascular Medical Institute
[7]Center for Metabolism and Mitochondrial Medicine
University of Pittsburgh School of Medicine, Pittsburgh, PA 15213, USA
[8]Co-first author
*Correspondence: raya@pitt.edu
http://dx.doi.org/10.1016/j.celrep.2016.04.060

SUMMARY

Inhalation of environmental antigens such as allergens does not always induce inflammation in the respiratory tract. While antigen-presenting cells (APCs), including dendritic cells and macrophages, take up inhaled antigens, the cell-intrinsic molecular mechanisms that prevent an inflammatory response during this process, such as activation of the transcription factor NF-κB, are not well understood. Here, we show that the nuclear receptor PPARγ plays a critical role in blocking NF-κB activation in response to inhaled antigens to preserve immune tolerance. Tolerance induction promoted mitochondrial respiration, generation of H_2O_2, and suppression of NF-κB activation in WT, but not PPARγ-deficient, APCs. Forced restoration of H_2O_2 in PPARγ-deficient cells suppressed IκBα degradation and NF-κB activation. Conversely, scavenging reactive oxygen species from mitochondria promoted IκBα degradation with loss of regulatory and promotion of inflammatory T cell responses in vivo. Thus, communication between PPARγ and the mitochondria maintains immune quiescence in the airways.

INTRODUCTION

Inhalation of antigen/allergen is a natural and spontaneous process, which normally maintains immune tolerance in the airways (Curotto de Lafaille et al., 2008; Khare et al., 2013, 2015; McMenamin et al., 1994; Ostroukhova et al., 2004). This process of tolerance prevents inflammatory immune responses to inhaled antigens that, in susceptible individuals, can lead to allergic diseases such as asthma (Lambrecht and Hammad, 2012). Immune tolerance also prevents autoimmune diseases and transplant rejections. Antigen-presenting cells (APCs) such as dendritic cells (DCs) play a central role in the decision-making process between immune activation and tolerance (Steinman, 2012). It is, therefore, important to understand the molecular mechanisms by which APCs mediate immune tolerance to be able to use their full potential for suppression of undesirable immune activation.

Recent literature highlights cross-talk between cellular metabolism and immune function (Odegaard et al., 2007; Tschopp, 2011). One example is metabolic syndrome, which is often associated with chronic unregulated inflammation in various organs (Odegaard et al., 2007; Tschopp, 2011). It is suggested that dysregulated production of reactive oxygen species (ROS) in mitochondria contributes to metabolic syndrome (James et al., 2012). More than 30 years ago, the ability of isolated mitochondria to produce the ROS H_2O_2 was demonstrated (Chance et al., 1979). Subsequent studies showed that H_2O_2 is generated by dismutation of superoxide by the action of a superoxide dismutase (SOD) within mitochondria (Forman and Kennedy, 1974; Loschen et al., 1974). These discoveries collectively established mitochondria as an important source of cellular H_2O_2. Given that mitochondria have emerged as important regulators of multiple cellular functions (Galluzzi et al., 2012), it seems equally plausible that regulated mitochondrial ROS production contributes to immune homeostasis.

Peroxisome proliferator-activated receptor gamma (PPARγ), a member of the nuclear receptor superfamily, not only promotes adipocyte differentiation and glucose homeostasis but also exerts anti-inflammatory effects (Wahli and Michalik, 2012). PPARγ deletion in myeloid cells was shown to impair generation of alternatively activated macrophages and induce insulin resistance,

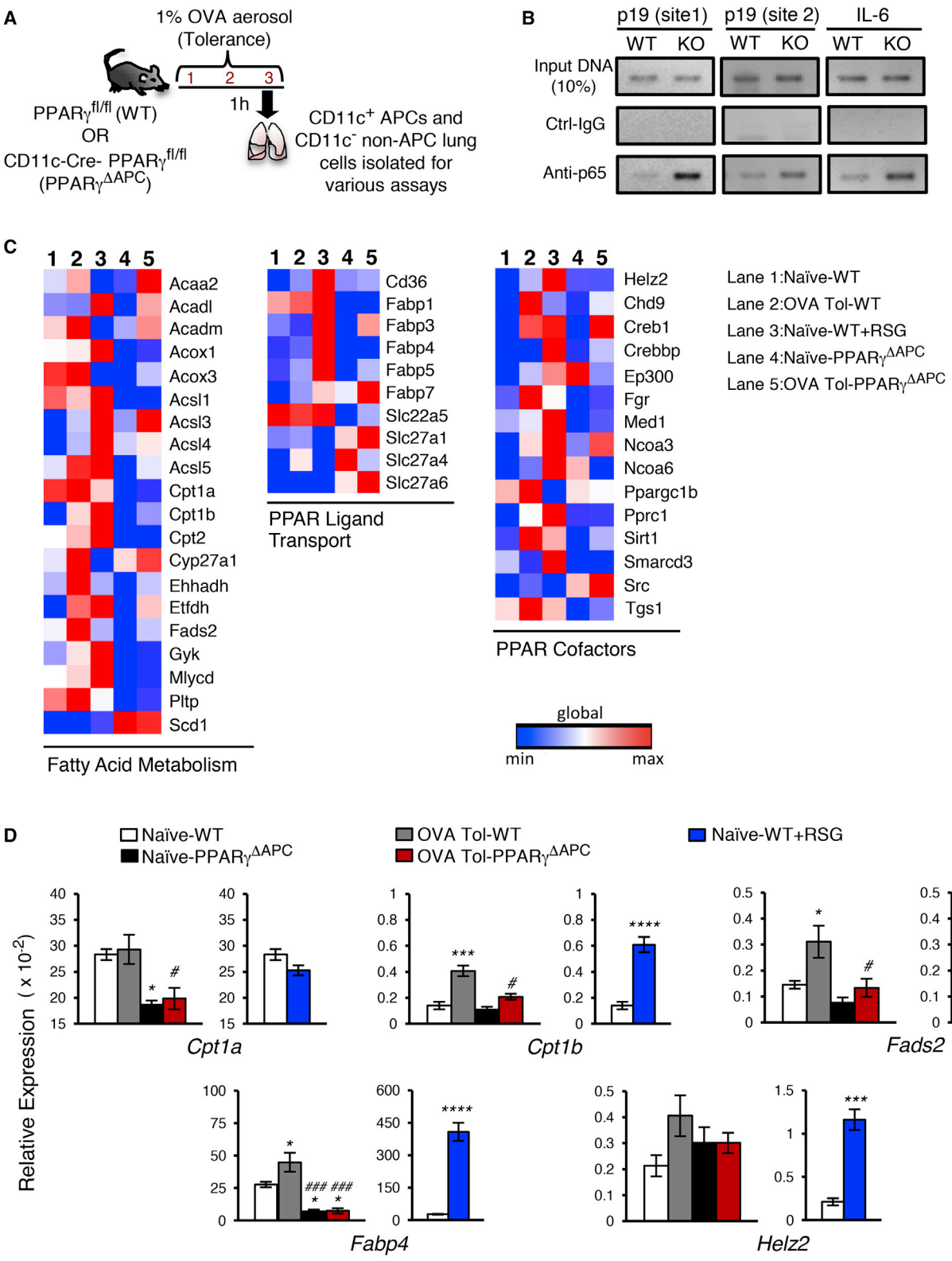

Figure 1. Inhaled Antigen-Activated PPARγ Regulates Genes Involved in the Regulation of Inflammation and Fatty Acid Metabolism

(A) Schematic describes the 3-day OVA-exposure protocol for tolerance.

(B) ChIP assay of p19 and IL-6 promoters in Tol CD11c$^+$ cells sorted from indicated conditions using anti-p65 and control antibodies is shown.

(legend continued on next page)

suggesting a beneficial role of PPARγ in controlling metabolic diseases such as type 2 diabetes (Odegaard et al., 2007; Tschopp, 2011). In the lung, PPARγ is expressed by multiple cell types including CD11c$^+$ cells, which include the APC DCs and macrophages (Belvisi et al., 2006). We recently reported that conditional deletion of PPARγ in the CD11c$^+$ APCs in mice induces an inflammatory response in the airways (Khare et al., 2015). However, the molecular mechanism by which PPARγ expression in CD11c$^+$ cells efficiently suppresses airway inflammation despite constant provocation of the lungs by environmental antigens remains poorly understood.

Here we show that, in the absence of PPARγ, NF-κB is recruited to the promoters of the pro-inflammatory cytokine genes, IL-6 and the p19 subunit of IL-23 in lung APCs, in keeping with increased production of these cytokines in these cells (Khare et al., 2015). Under tolerizing conditions, PPARγ-sufficient CD11c$^+$ cells displayed higher oxygen consumption rate (OCR) than PPARγ-deficient CD11c$^+$ cells, which was sensitive to Cpt1 blockade. Using two independent H_2O_2 detection methods, we identified H_2O_2 in wild-type (WT), but not PPARγ-deficient, cells from tolerized mice, which involved mitochondrial Complex I, but not Complex III, activity. PPARγ was essential for increased SOD activity in the cells. Forced restoration of H_2O_2 in PPARγ-deficient cells suppressed IκBα degradation. Conversely, use of a mitochondrially targeted H_2O_2 scavenger, Mito-Tempo (Dikalova et al., 2010; Murphy, 1997), promoted IκBα degradation, and airway tolerance was replaced by an inflammatory response, as observed in mice devoid of PPARγ in CD11c$^+$ cells (Khare et al., 2015). Taken together, these findings establish a communication axis among the nucleus, mitochondria, and the cell cytoplasm to prevent unnecessary immune activation in the airways under conditions of constant antigenic provocation.

RESULTS

Increased Recruitment of NF-κB to Promoters of Pro-inflammatory Cytokine Genes in PPARγ-Deficient CD11c$^+$ Cells and PPARγ-Dependent Expression of Genes Involved in Fatty Acid Metabolism

We recently reported that conditional deletion of *PPARγ* in CD11c$^+$ cells, which include the APC DCs and macrophages in the lungs, abolishes tolerance in the airways induced by low doses of inhaled antigen with induction of inflammation, although the underlying molecular mechanism was not described (Khare et al., 2015). These *CD11c-Cre*$^{+/-}$*-PPARγ*$^{fl/fl}$ mice (referred to hereafter as PPARγ$^{\Delta APC}$ mice) showed a minimal change in the numbers of lung DCs as compared to the control *PPARγ*$^{fl/fl}$ mice (referred to hereafter as WT mice), but they showed enhanced expression of pro-inflammatory cytokine genes under tolerizing conditions in all CD11c$^+$ cells that included CD103$^+$ DCs, CD103$^-$ DCs, and macrophages (Khare et al., 2015). Since NF-κB is a central regulator of expression of pro-inflammatory cytokine genes (Hayden and Ghosh, 2008; Pasparakis, 2009), we investigated whether deletion of PPARγ in CD11c$^+$ cells aberrantly triggers NF-κB activation in response to a low dose of inhaled antigen, which normally maintains airway tolerance (Khare et al., 2013, 2015; Ostroukhova et al., 2004). We used a shorter protocol for tolerance induction, which involved exposure of the mice to 3 consecutive days of aerosolized ovalbumin (OVA) (Figure 1A) instead of 10 days as previously described by us (Khare et al., 2013, 2015; Ostroukhova et al., 2004). Both protocols blunted induction of airway inflammation to the same degree when tested for tolerance induction by subsequently immunizing the mice with OVA plus adjuvant and then repeatedly challenging by aerosolized OVA (Figure S1A). In both protocols, we observed minimal recruitment of the p65 subunit (Rel A) of NF-κB to the different NF-κB sites in the p19 and IL-6 promoters in PPARγ-sufficient cells, while p65 recruitment was readily detectable when cells were PPARγ deficient (Figures 1B and S1B).

Of note, in a study published recently in which PPARγ was similarly deleted in CD11c$^+$ cells, a complete arrest in the development of alveolar macrophages (AMs) characterized as CD11c$^+$CD11b^{lo} cells in bronchoalveolar lavage (BAL) and lung cells was reported (Schneider et al., 2014). Instead, a significant increase in CD11c^{hi} cells that were CD11b^{hi}, autofluorescent, and expressed F4/80 was noted; these cells were described as AM-like cells (Schneider et al., 2014). Using a similar AM characterization strategy, we found that, while CD11c^{hi}CD11b^{hi} AM-like cells are present in BAL and lung cells of PPARγ$^{\Delta APC}$ mice generated by us (Figure S2A), CD11c$^+$CD11b^{lo} cells resembling AMs were only reduced by ~50% in these mice (Figure S2A), unlike their complete absence in the *PPARγ* conditional knockouts described in the earlier study (Schneider et al., 2014). We then focused on Siglec-F expression on CD11c$^+$F4/80$^+$ cells, the co-expression of these molecules being restricted to only macrophages in the lungs. We observed a slight reduction in CD11c$^+$F4/80$^+$ cells in the lungs of PPARγ$^{\Delta APC}$ mice as compared to those in WT mice (Figure S2B). When gated on these cells, 15% were CD11b^{hi}Siglec-F$^+$ cells in PPARγ$^{\Delta APC}$ mice as compared to 5% in WT mice with no downregulation of Siglec-F expression in any subset, unlike what was observed in the earlier study (Schneider et al., 2014). Thus, collectively, the mice used by us had no difference in number of CD11c$^+$ autofluorescence^{lo} DCs or CD11c$^+$ autofluorescence^{hi} macrophages (AM and AM-like cells together) (Khare et al., 2015). The partial reduction in AM numbers in the PPARγ$^{\Delta APC}$ mice (Khare et al., 2015) did not explain either the increase in expression of pro-inflammatory cytokine genes in the CD11c$^+$ cells derived from these mice or the inability of these mice to support Treg

(C) Heatmap representation of PPAR target array experiments for the indicated genes clustered based on function. mRNA was isolated from CD11c$^+$ cells from naive (lane 1), tolerized (lane 2), and ex vivo RSG-treated cells from WT mice (lane 3) and also from naive (lane 4) and tolerized PPARγ$^{\Delta APC}$ (lane 5) mice.
(D) Graphical representation of relative expression in CD11c$^+$ cells of indicated genes in specific groups present in the PPAR target array. Data shown are mean ± SEM and are representative of two independent experiments (n = 3–4 mice/group). One-way ANOVA with Tukey's post hoc test was used for comparisons among multiple groups; *$p < 0.05$, ***$p < 0.001$, and ****$p < 0.0001$ reflect comparisons to expression in naive PPARγ$^{fl/fl}$ and #$p < 0.05$ and ###$p < 0.001$ correspond to comparisons with OVA tol PPARγ$^{fl/fl}$.
See also Figures S1, S2, and S3.

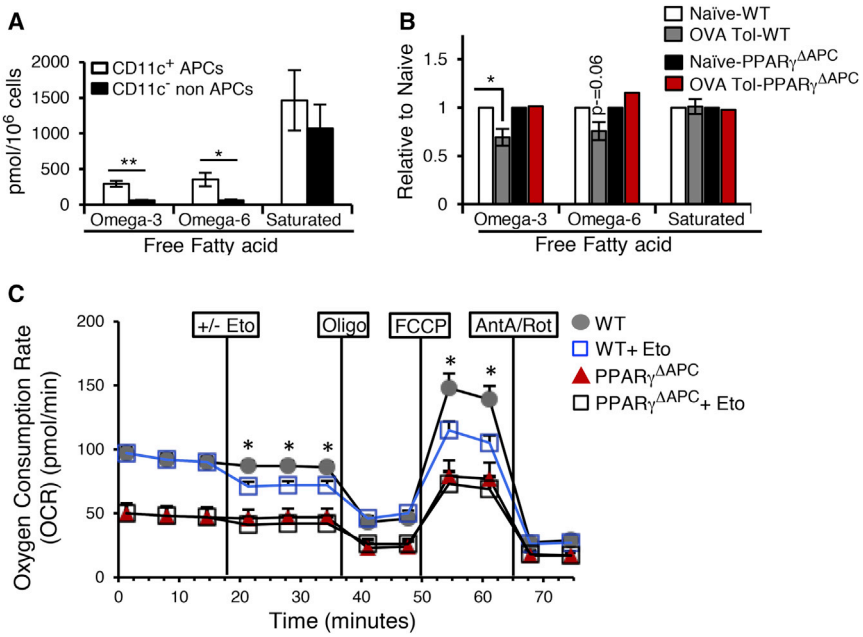

Figure 2. Antigen-Activated PPARγ Regulates Fatty Acid Metabolism

(A) Total omega-3, omega-6, and saturated FFA quantification (pmol/10^6 cells) as estimated by GC-MS analysis performed on CD11c$^+$ APCs and CD11c$^-$ B220$^-$ non-APCs sorted from the lungs of naive WT mice. Data shown are composite of three independent experiments and represent mean values ± SEM.

(B) Presence of omega-3, omega-6, and saturated FFAs in CD11c$^+$ cells sorted from the lungs of naive and tolerized WT and PPARγ$^{\Delta APC}$ mice as observed in two independent experiments, expressed as fold change (relative to naive of the respective strain). Data shown are composite of two independent experiments and represent mean values ± SD.

(C) OCR of CD11c$^+$ cells isolated from tolerized WT and PPARγ$^{\Delta APC}$ mice was measured at the basal level and then after sequential treatment with DMEM/200 μM Eto followed by 1 μM Oligo, 1.5 μM FCCP, and 0.1 μM Rot plus 1 μM Ant A using the XF-96 Seahorse system. The assay is representative of two independent experiments, run in triplicates, and shown as mean values ± SEM (*$p < 0.05$ and **$p < 0.01$).

development in response to tolerance-inducing conditions (Khare et al., 2015). Further, the increased presence of CD11b^{hi} macrophages in the lungs of the *PPARγ* conditional knockout mice suggested a shift in the population toward an activated phenotype (Guth et al., 2009; Stríz et al., 1993), as also was suggested by the increased production of cytokines such as IL-6 and the p19 subunit of IL-23 by these cells (Khare et al., 2015).

Our next task was to determine how the presence of PPARγ blocks NF-κB recruitment to the promoters of cytokine genes in CD11c$^+$ cells. PPARγ-mediated immune regulation requires activation by either synthetic agonists like thiazolidinediones (TZDs) or by endogenous ligands such as fatty acids. Our model did not employ any synthetic ligand, and yet involvement of PPARγ in regulating the activation status of CD11c$^+$ cells was evident. Using a focused gene array, we compared the mRNA expression profile of PPAR-regulated genes in the following different sets of lung CD11c$^+$ cells: those stimulated by the TZD rosiglitazone (RSG) ex vivo, and those isolated from naive or antigen (OVA)-tolerized (OVA-Tol) WT or PPARγ$^{\Delta APC}$ mice (Figures 1C, 1D, and S3). The enzymes Cpt1a and Cpt1b are involved in fatty acid translocation across the mitochondrial membrane, and expression of the former is typically higher in immune cells (Wakil and Abu-Elheiga, 2009). The expression of *Cpt1a* was significantly reduced in PPARγ-deficient cells as compared to that in WT cells (Figures 1C and 1D). Albeit expressed at a lower level, the relative increase in *Cpt1b* expression also was less in cells without PPARγ (Figures 1C and 1D). Fatty acid desaturase-2 (Fads-2) is an important enzyme that catalyzes the generation of polyunsaturated fatty acids (PUFAs) (Guillou et al., 2010). In response to inhaled antigen, the increase in *Fads2* expression was higher in WT cells as compared to that in PPARγ-deficient cells. As expected from previous publications, mRNA level of fatty acid-binding protein-4 (*Fabp4*) increased several fold in RSG-treated cells (Odegaard et al., 2007), and the expression of *helicase with zinc finger 2* (*helz2*), which is a co-activator of PPARγ and promotes optimal expression of *Fabp4* (Katano-Toki et al., 2013), also was increased (Figures 1C and 1D). The differential response of cells to inhaled antigen versus RSG, both mediated by PPARγ, suggested a distinct molecular mechanism of PPARγ action under conditions of tolerance. Since Fabp4 binds and sequesters free fatty acids (FFAs) in the cytoplasm of cells (Furuhashi and Hotamisligil, 2008), and its expression was not upregulated in the CD11c$^+$ cells from tolerized mice to the extent that it was upon RSG treatment, we next examined the status of FFAs in the CD11c$^+$ cells.

Lung CD11c$^+$ cells as well as CD11c$^-$ cells (minus B cells) sorted from naive and tolerized WT and PPARγ$^{\Delta APC}$ mice were subjected to FFA analysis employing gas chromatography coupled with mass spectrometry (GC-MS) (Figures 2A and 2B) (Quehenberger et al., 2011). CD11c$^+$ APCs from naive WT mice contained significantly higher levels of free ω-3 and ω-6 PUFAs compared to CD11c$^-$ non-APCs, in which these FFAs were barely detectable (Figure 2A). The levels of free saturated fatty acids were, however, comparable between CD11c$^+$ APCs and CD11c$^-$ non-APCs (Figure 2A). Under PPARγ-sufficient conditions, the levels of both ω-3 and ω-6 PUFAs were lower in CD11c$^+$ cells from tolerized mice as compared to cells from naive mice, with the decrease in ω-3 PUFAs reaching statistical significance. However, the levels of saturated fatty acids were similar in cells from naive and tolerized WT mice (Figure 2B). In accordance with the gene expression data showing lower *Cpt1* expression in PPARγ-deficient cells, there was no decrease in ω-3 and ω-6 PUFAs in these cells isolated from tolerized PPARγ$^{\Delta APC}$ mice (Figure 2B).

We next assessed OCR of CD11c$^+$ cells isolated from tolerized WT and PPARγ$^{\Delta APC}$ mice. OCR was measured at the basal level, and then one batch of cells in both groups was treated with etomoxir (Eto) and then sequentially treated with oligomycin (Oligo),

carbonyl cyanide 4-(trifluoromethoxy)phenylhydrazone (FCCP), and rotenone plus antimycin (Ant A + Rot). Basal OCR in WT cells was inhibited upon treatment with Eto, a specific inhibitor of Cpt1 (Wolf and Brenner, 1988). PPARγ-deficient CD11c$^+$ cells showed lower OCR overall as compared to PPARγ-sufficient cells, which was unchanged upon Eto treatment (Figure 2C). The maximal OCR reached after FCCP injection of WT cells previously treated with Eto remained lower than those maintained without Eto, suggesting fatty acid oxidation (FAO) to be an important component of OCR in tolerized WT cells. These results suggested that conditions of tolerance or even basal conditions that regulate immune homeostasis favor maintenance of a relatively high level of endogenous PPARγ ligands, such as PUFAs in lung APCs, but not in non-APCs. Also, the lower levels of free PUFAs in CD11c$^+$ cells from tolerized WT mice combined with higher *Fads2* and *Cpt1* expression together with higher Eto-sensitive OCR in these cells suggested β-oxidation of fatty acids in mitochondria with increased mitochondrial ROS production in the cells.

Increased Mitochondrial H_2O_2 Production under Conditions of Tolerance

The fact that PUFAs are not only ligands of PPARγ but also are substrates for mitochondrial electron transport (Lombardi et al., 2008; Nethery et al., 2000) led us to examine the production of ROS in lung CD11c$^+$ cells. When generated in small quantities via the mitochondrial electron transport chain (mETC) (Chance et al., 1979), H_2O_2 has been shown to be important for tissue homeostasis (Poole et al., 1997). Surprisingly, the role of ROS in regulation of immune homeostasis, including activation of important transcription factors such as NF-κB under physiological conditions, remains unclear. H_2O_2 is a diffusible molecule and can be assayed in the extracellular medium by the Amplex Red assay, a suitable method for quantitation of H_2O_2 production (Kalyanaraman et al., 2012). H_2O_2 generated in CD11c$^+$ cells from tolerized PPARγ$^{fl/fl}$ mice was greater when compared to cells from naive mice (Figure 3A). Inhibition of H_2O_2 generation in PPARγ-sufficient CD11c$^+$ cells from tolerized mice by Rot, a specific inhibitor of mitochondrial complex I (Figure 3A) (Lombardi et al., 2008; Murphy, 2009), but not by Ant A, a specific inhibitor of complex III (Figure 3A) or L-NAME (NOS2 inhibitor) (Xia et al., 1996), confirmed the involvement of the mETC in increased H_2O_2 levels in response to antigen (Figure 3A). Furthermore, inhibition by Rot suggested the involvement of reverse electron transport (RET) in mitochondrial ROS generation (Murphy, 2009). In other studies in skeletal muscle cells, mitochondrial H_2O_2 generation induced by PUFA (arachidonic acid) also was inhibited by Rot (Lombardi et al., 2008). We also observed that PPARγ-sufficient CD11c$^+$ cells treated with RSG did not generate H_2O_2 (Figure 3A), which reaffirmed that RSG-mediated and low-dose antigen-mediated PPARγ activation induce different responses in the CD11c$^+$ cells. Figure 3A shows specificity of the mETC inhibitors with selective inhibition of complex I by Rot and of complex III by Ant A (Shiva et al., 2007).

We next assessed whether the increase in H_2O_2 production from CD11c$^+$ cells from tolerized WT mice depends on PPARγ, which was found to be the case (Figure 3B). Essentially, similar results were obtained by imaging when the boronate compound peroxyfluor-6 acetoxymethyl ester (PF6-AM), a selective fluorescent detector of H_2O_2 (Basu et al., 2014; Dickinson et al., 2011; Lin et al., 2013), was used with H_2O_2 readily detected in CD11c$^+$ cells from WT, but not PPARγ-deficient, cells (Figure 3C). Similar results were obtained when the mice were exposed to a different allergen, Derp1, of house dust mite (Cates et al., 2004) (Figure 3C), demonstrating the generality of the effect of PPARγ deficiency in CD11c$^+$ cells on H_2O_2 generation in the cells. The results described above raised the question of how PPARγ promotes H_2O_2 generation in the CD11c$^+$ cells. Cellular H_2O_2 is generated following dismutation of superoxide radical generated during mitochondrial electron transport by SOD enzymes (Buettner, 2011). The expression of both *MnSOD* (SOD2), which is targeted to mitochondria, and of *CuZnSOD* (SOD1), which is cytosolic, at both mRNA and protein levels, was reduced in PPARγ-deficient cells compared to WT cells (Figure 3D). PPARγ-sufficient, but not PPARγ-deficient, CD11c$^+$ cells showed increased SOD activity (Figure 3E). PPARγ-induced SOD activity under tolerizing conditions in WT cells can, therefore, be expected to cause an increase in cytosolic H_2O_2 level due to diffusion of H_2O_2 across the mitochondrial membrane (Brand, 2010).

We next examined the morphology of mitochondria in CD11c$^+$ cells derived from naive and tolerized WT and PPARγ$^{\Delta APC}$ mice by staining the mitochondrial membrane with Tom20. Mitochondria are extremely dynamic organelles that fragment and fuse continuously; the morphology of mitochondria (fragmented versus extensive fused networks) strongly influences function (da Silva et al., 2014). Mitochondrial abundance was measured using confocal microscopy followed by three-dimensional surface rendering and calculation of mitochondrial volume (abundance). Mitochondrial fragmentation was assessed using the sphericity parameter. The closer the sphericity value is to 1, the more spherical and fragmented the mitochondria. The average sphericity in our samples was low, ranging around 0.5, indicating that the mitochondria were highly networked. Both volume and sphericity calculations showed no difference whether cells were examined from WT or PPARγ-deficient cells (Figures 3F and S4). Similar data were obtained by quantifying the mtDNA copy number in WT and PPARγ-deficient cells (Figure 3G). These observations ruled out a difference in mitochondrial abundance or health between the WT and PPARγ$^{\Delta APC}$ mice as contributing to the increased inflammatory phenotype of the latter and instead focused our attention on regulation of gene expression by H_2O_2.

PPARγ Prevents NF-κB Activation in Tolerized Mice

The physiological relevance of the effects of high concentrations of H_2O_2 on NF-κB activation in vitro is difficult to ascertain without in vivo supportive evidence (Oliveira-Marques et al., 2009). Unlike most studies that have shown mild NF-κB activation in response to large doses of H_2O_2 (Oliveira-Marques et al., 2009), one prior study using mouse alveolar epithelial cells showed that H_2O_2 can inhibit NF-κB activation by limiting IKK phosphorylation (Korn et al., 2001). Consistent with this finding, we observed greater IKK phosphorylation in tolerized PPARγ-deficient CD11c$^+$ cells compared to PPARγ-sufficient cells (Figure 4A), the former having lower H_2O_2 levels (Figures 3B and 3C).

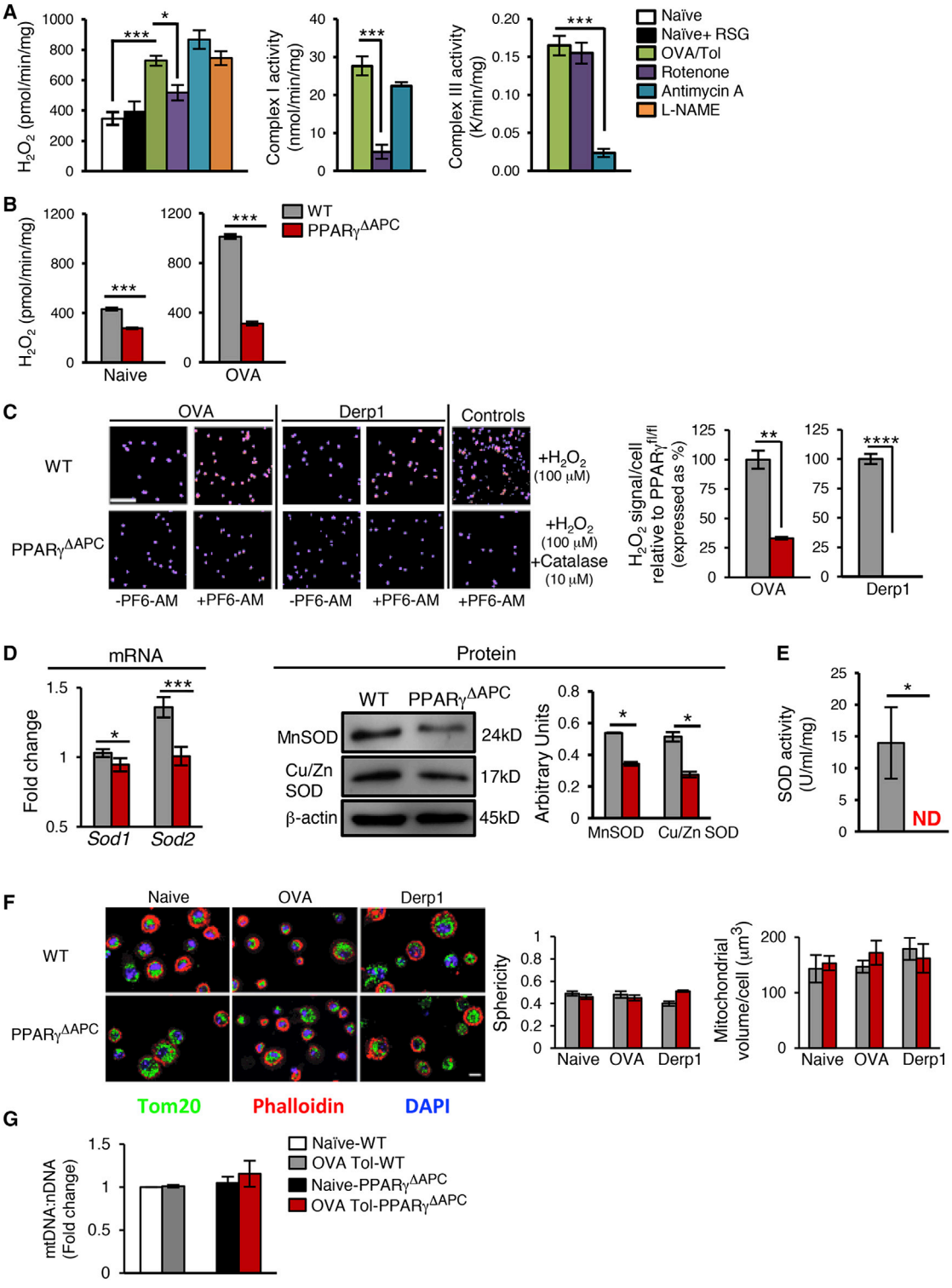

Figure 3. PPARγ Expression Regulates Mitochondrial ROS Generation

(A) Amplex Red assay was used to quantitate H_2O_2 generation in sorted lung CD11c$^+$ cells from naive WT mice in the presence or absence of RSG (10 μM) and tolerized WT mice in the presence or absence of Rot (10 μM), Ant A (100 μM), or L-NAME (50 μM). Complex I and complex III activities were measured to assess specificity and dose efficiency of Rot and Ant A, respectively.

(B) Quantification of H_2O_2 generation in sorted lung CD11c$^+$ cells from naive and tolerized WT and PPARγ$^{\Delta APC}$ mice. Data for (A) and (B) represent one of three independent experiments and are shown as mean ± SEM.

(legend continued on next page)

IKK mediates phosphorylation of specific Ser residues in IκBα, leading to ubiquitination and proteasomal degradation (reviewed in Karin and Ben-Neriah, 2000). In accordance with the IKK phosphorylation data, a lower expression level of IκBα in the cytoplasmic extracts of PPARγ-deficient CD11c$^+$ cells was found as compared to that in control CD11c$^+$ cells. In lung CD11c$^-$ cells, in which PPARγ was not deleted, the level of IκBα was comparable between PPARγ$^{\Delta APC}$ and WT mice (Figure 4A). Conversely, a higher expression of c-rel and the p65 subunit of NF-κB (RelA) was observed in the nuclear extracts of PPARγ-deficient CD11c$^+$ cells when compared to control extracts (Figure 4B). Similar observations were made when mice were exposed to Derp1 (Figure 4C), demonstrating the generality of effect of PPARγ deficiency in CD11c$^+$ cells on NF-κB activation. Both chymotrypsin-like and trypsin-like proteasomal activities were similar in CD11c$^+$ cells from PPARγ$^{\Delta APC}$ and WT mice irrespective of whether cells were isolated from naive or OVA-exposed mice (Figure S5A), ruling out a difference in proteasomal activity between PPARγ-sufficient and PPARγ-deficient cells as playing any role in differential NF-κB activation in these cells.

If PPARγ-dependent H_2O_2 generation indeed inhibits phosphorylation of IκBα, we hypothesized that incubation of PPARγ-deficient CD11c$^+$ cells with 2,3-dimethoxy-1,4-naphthoquinone (DMNQ), a non-thiol-capturing and non-alkylating redox-cycling quinone that causes continuous intracellular generation of H_2O_2 (Parry et al., 2009), would reverse the effects on IκBα. Importantly, forced generation of H_2O_2 using DMNQ does not require SOD, which provided an opportunity to bypass PPARγ. Indeed, DMNQ treatment resulted in increased intracellular H_2O_2 levels (Figure S5B), reducing pIκBα and increasing IκBα levels compared to untreated cells (Figure 4D). DMNQ caused a similar differential in pIκBα and IκBα, albeit lower in magnitude, in cells from tolerized WT mice that, to begin with, harbored a higher level of H_2O_2 (Figure 4D). Correspondingly, reduced nuclear translocation of p65 was observed in DMNQ-treated cells compared to untreated cells (Figure 4D).

To further investigate a causal relationship between reduced H_2O_2 and heightened NF-κB activation in the CD11c$^+$ cells, we co-cultured CD11c$^+$ DCs from tolerized CD11c-specific PPARγ-deficient and -sufficient mice with carboxyfluorescein succinimidyl ester (CFSE)-labeled Treg-depleted OT-II CD4$^+$ T cells in the presence of OVA peptide, and we assessed T cell proliferation. The PPARγ-deficient cells induced better T cell proliferation compared to WT cells, as determined by quantitation of the percentage of CFSE$^+$ cells in each population of divided cells (Figure 5A). T cell proliferation induced by the PPARγ-deficient CD11c$^+$ cells was drastically inhibited by pre-treatment of the DCs with the specific inhibitor of IκBα phosphorylation, BAY 11-7082 (Figures 5B and S6). A significant decrease in the level of IL-2 also was observed in co-cultures stimulated with DCs pre-treated with BAY-117082 (Figure 5C).

Scavenging Mitochondrial ROS Promotes NF-κB Activation and Impairs Airway Tolerance

To further confirm the specific role of mitochondrial ROS in the suppression of NF-κB activation, we made use of the mitochondrially targeted ROS scavenger Mito-TEMPO (Dikalova et al., 2010; Murphy, 1997). As shown in Figure 6A, use of Mito-TEMPO reduced H_2O_2 production from the CD11c$^+$ cells isolated from C57/BL6J tolerized mice. Next we used Mito-TEMPO in vivo to demonstrate the importance of mitochondrial ROS in blocking NF-κB activation and expression of pro-inflammatory cytokine genes during tolerance, thereby favoring Treg generation and immune suppression. Mito-TEMPO was instilled into mice using an osmotic pump and exposed the mice to aerosolized OVA. Lung CD11c$^+$ cells isolated from mice that received Mito-TEMPO showed a higher level of pIκBα and a lower level of IκBα as compared to those that received saline (Figure 6B). While the results of these experiments do not exclude a role for other cellular superoxide-generating systems (including NADPH oxidase), in aggregate, our data demonstrate that mitochondrially derived H_2O_2 contributes significantly to NF-κB inhibition.

Since Foxp3 induction in adoptively transferred naive CD4$^+$ T cells is severely impaired in CD103 DC-deficient Batf3$^{-/-}$ mice (Khare et al., 2013), we asked whether quenching of mitochondrial ROS by Mito-TEMPO in vivo, which would cause NF-κB activation in all DCs including CD103$^+$ DCs, would similarly affect Foxp3 induction in naive CD4$^+$ T cells. Treatment with Mito-TEMPO blunted Foxp3 induction in adoptively transferred CD4$^+$CD25$^-$ T cells from OT-IIxThy1.1 mice (Figure 6C). Conversely, we detected increased expression of the pro-inflammatory cytokine IL-23p19 (Figures 6D and 6E) in CD103$^+$ DCs isolated from Mito-TEMPO-treated tolerized mice compared to controls. Compared to vehicle-treated controls, tolerized mice that received Mito-TEMPO showed a significant increase in neutrophil infiltration and a smaller increase in eosinophil infiltration in the airways when challenged in the inflammation model (Figure 6F). The accompanying CD4$^+$ T cell response

(C) Intracellular H_2O_2 detection in sorted lung CD11c$^+$ cells from tolerized WT and PPARγ$^{\Delta APC}$ mice using the H_2O_2-specific probe PF6-AM. During the incubation with PF6-AM, OVA (10 μg/ml) or Derp 1 (0.5 μg/ml) was included. In the absence of antigen in vitro, a similar profile was obtained with lower signal intensity in the WT cells and none detected in the PPARγ-deficient cells (data not shown). As a positive control, exogenous H_2O_2 (100 μM) was added to the CD11c$^+$ cells in vitro ± catalase (10 μM). Representative immunofluorescence images (left) and fluorescence quantification (right) represent cytosolic H_2O_2 signal per cell per field (five to six fields chosen randomly using DAPI as a guide and then assessed for PF6-AM-specific signal). Scale bar, 100 μm and magnification 20×. Bar graphs show data as mean values ± SEM.

(D and E) Lung CD11c$^+$ cells from tolerized WT and PPARγ$^{\Delta APC}$ mice were analyzed for (D) MnSOD and Cu/ZnSOD mRNA (left panel) and protein expression (right panel) and (E) SOD activity. Data are shown as mean values ± SD.

(F) Representative immunofluorescence images (left) and sphericity and mitochondrial volume/cell estimation (right) of lung CD11c$^+$ cells stained with Tom20 (green), DAPI (blue), and phalloidin (red) are shown. Scale bar, 10 μm; magnification 60×.

(G) Quantification of mtDNA and nuclear DNA (nDNA) in purified lung CD11c$^+$ cells from naive and tolerized WT and PPARγ$^{\Delta APC}$ mice. Data in panels (F) and (G) represent one of two independent experiments and are shown as mean values ± SD. ND, not detected; NS, not significant; *$p < 0.05$, ***$p < 0.001$, ****$p < 0.0001$. See also Figure S4.

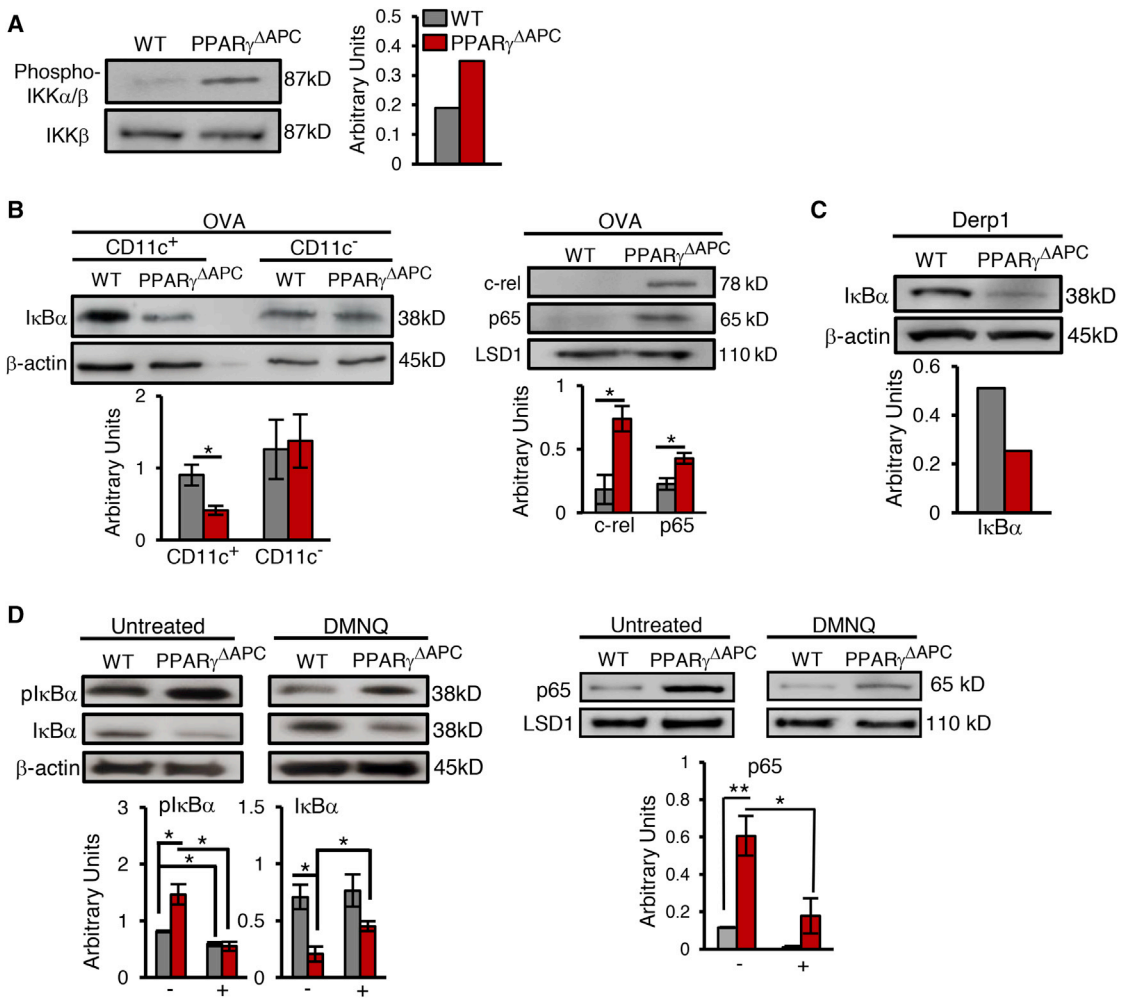

Figure 4. Absence of Mitochondrial ROS Promotes NF-κB Activation

(A–D) Representative western blot and densitometry quantification to detect expression of (A) phospho IKKα/IKKβ levels in sorted CD11c$^+$ cells; (B) IκBα in cytoplasmic extracts and c-rel, p65 subunit (RelA) of NF-κB in nuclear extracts prepared from lung CD11c$^+$ and CD11c$^-$ cells from PPARγ$^{\Delta APC}$ and WT mice 1 hr after the last exposure to OVA; (C) IκBα in lung CD11c$^+$ cells sorted from PPARγ$^{\Delta APC}$ and WT mice 1 hr after the last exposure to Derp1; and (D) phospho IκBα (pIκBα) and total IκBα levels in whole-cell extract and p65 levels in nuclear extracts from lung CD11c$^+$ cells (sorted from tolerized mice), cultured for 1 hr in the presence or absence of DMNQ (200 μM). For all western blot analyses, expression of β-actin and LSD1 is shown as loading controls for cytoplasmic and nuclear extracts, respectively, and densitometric quantification is combined data from two independent experiments represented as mean ± SD. ND, not detected; *$p < 0.05$, **$p < 0.01$.

See also Figure S5.

showed a prominent increase in IL-17 expression accompanied by an increase in IFN-γ expression (Figure 6G). Therefore, results obtained with Mito-TEMPO treatment of mice were in close agreement with those derived using PPARγ$^{\Delta APC}$ mice (Khare et al., 2015), thereby demonstrating that a major mechanism by which PPARγ regulates immune tolerance is by controlling mitochondrial ROS generation.

DISCUSSION

Our study highlights a previously unappreciated function of PPARγ in regulating immune tolerance induced by low doses of inhaled antigen by invoking mitochondrial metabolism in lung APCs. We show that PPARγ prevents nuclear translocation of NF-κB, limiting binding to target sites in the promoters of pro-inflammatory cytokine genes. Use of a targeted gene array revealed differential expression of enzymes involved in mitochondrial FAO between WT and PPARγ-deficient cells. PPARγ was required for optimal *Cpt1a* and *Cpt1b* mRNA expression in CD11c$^+$ cells, Cpt1 proteins being required for FFA translocation to mitochondria. PPARγ also promoted expression of *Fads2* in response to inhaled antigen, Fads-2 being shown to catalyze de novo generation of PUFAs. We show that the OCR of WT cells from tolerized mice is inhibited by blockade of Cpt1 and is substantially reduced in the absence of PPARγ. We provide evidence of mitochondrial respiration involving complex I for

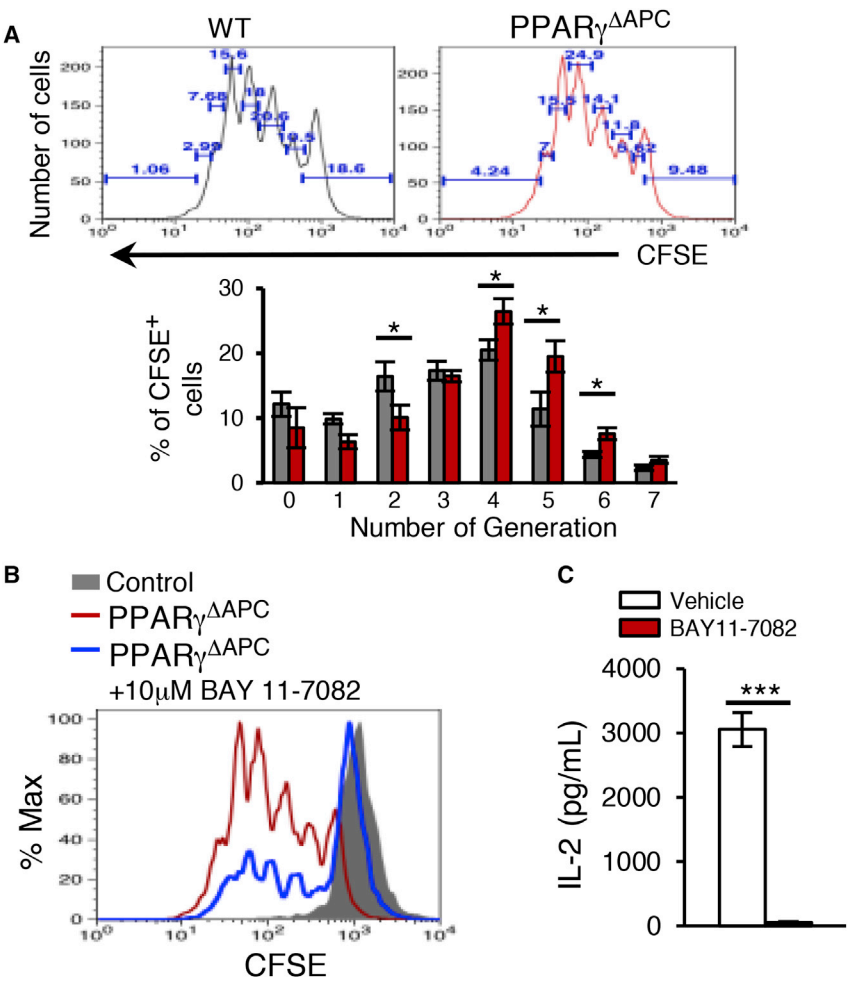

Figure 5. Absence of PPARγ in CD11c$^+$ DCs Promotes T cell Proliferation via NF-κB Activation

CFSE-labeled Treg-depleted OT-II splenic CD4$^+$ T cells were stimulated with either vehicle or BAY11-7082 (10 μM) pre-treated CD11c$^+$ DCs sorted from tolerized PPARγ$^{\Delta APC}$ and WT mice.

(A) T cell proliferation was assessed after 72 hr by estimating CFSE dilution using flow cytometry, and number of cells per generation was calculated.

(B) Overlay plot showing T cell proliferation as CFSE dilution when stimulated in presence of either vehicle or BAY11-7082 (10 μM) pre-treated CD11c$^+$ DCs sorted from tolerized PPARγ$^{\Delta APC}$ mice. Data shown are representative of three independent experiments.

(C) Expression of IL-2 was assessed in the PPARγ$^{\Delta APC}$ DC-T cell co-culture supernatant by ELISA. Data for (A) and (C) are shown as mean values ± SEM and composite of three independent experiments. *p < 0.05, ***p < 0.00.

See also Figure S6.

increased H_2O_2 generation in response to inhaled antigen in WT cells, which inhibited IκBα phosphorylation/NF-κB activation in these cells. It is interesting to note that mitochondrial complex III activity causing increased ROS generation has been associated with IL-2 production and NF-AT activation in T cells (Sena et al., 2013). Loss of PPARγ in the CD11c$^+$ cells led to undetectable SOD activity, explaining reduced H_2O_2 generation in the cells. Scavenging of mitochondrial ROS induced IκBα phosphorylation and promoted expression of cytokine genes, which favored T helper responses and inhibited Treg development with the loss of immune tolerance.

Our gene expression data and FFA analyses collectively suggest that an important task of PPARγ is to promote mitochondrial oxidation of PUFAs in lung APCs. It is important to note that, in the CD11c$^+$ cells during inflammation, we have detected lower expression of PPARγ (Khare et al., 2015). Thus, although PUFAs are present in CD11c$^+$ cells under conditions of inflammation (data not shown), lower levels of PPARγ translating into lower SOD activity would prevent an increase in H_2O_2 level in these cells, promoting NF-κB activation. The relevance of weak NF-κB activation by H_2O_2 observed in in vitro studies by treating cell lines with H_2O_2 or by using antioxidants such as N-acetyl cysteine (NAC) or pyrrolidine dithiocarbamate (PDTC) has been a subject of considerable debate (Oliveira-Marques et al., 2009). The positive effect of H_2O_2 on NF-κB activation observed in these studies has been largely cell type dependent, and, in some studies, it showed no evidence of IκBα degradation but instead involved tyrosine phosphorylation and dissociation of IκBα from NF-κB (Béraud et al., 1999). Also, reassessment of the effects of NAC and PDTC showed that they attenuated NF-κB activation independent of their antioxidant function.

Limited information exists about the role of H_2O_2 in the immune system. Our data show that PPARγ-deficient CD11c$^+$ cells from antigen-exposed mice have undetectable SOD activity and a lower H_2O_2 level. A peroxisome proliferator-response element (PPRE) was identified previously in the promoter of the CuZnSOD gene (Yoo et al., 1999). In addition, cardiac PPARγ was shown to be important for the expression of MnSOD (Ding et al., 2007). An increase in mitochondrial H_2O_2 level mediated by PPARγ-promoted SOD activity would result in increased cytosolic H_2O_2 level due to free diffusion of H_2O_2 across the mitochondrial membrane, resulting in phosphorylation and ultimately degradation of IκBα. Interestingly, SOD inactivation has been associated with asthma pathophysiology (Comhair et al., 2005). Our study suggests that, under ambient levels of exposure to environmental antigens, the PPARγ-dependent increase in H_2O_2 serves a prophylactic function by blocking NF-κB activation and its nuclear translocation, thereby preventing its recruitment to cytokine promoters. However, we propose that, with the use of next-generation TZDs with minimum side effects, PPARγ also can be utilized therapeutically, once inflammation is induced and NF-κB is recruited to target promoters where transrepression functions of PPARγ involving PPARγ SUMOylation

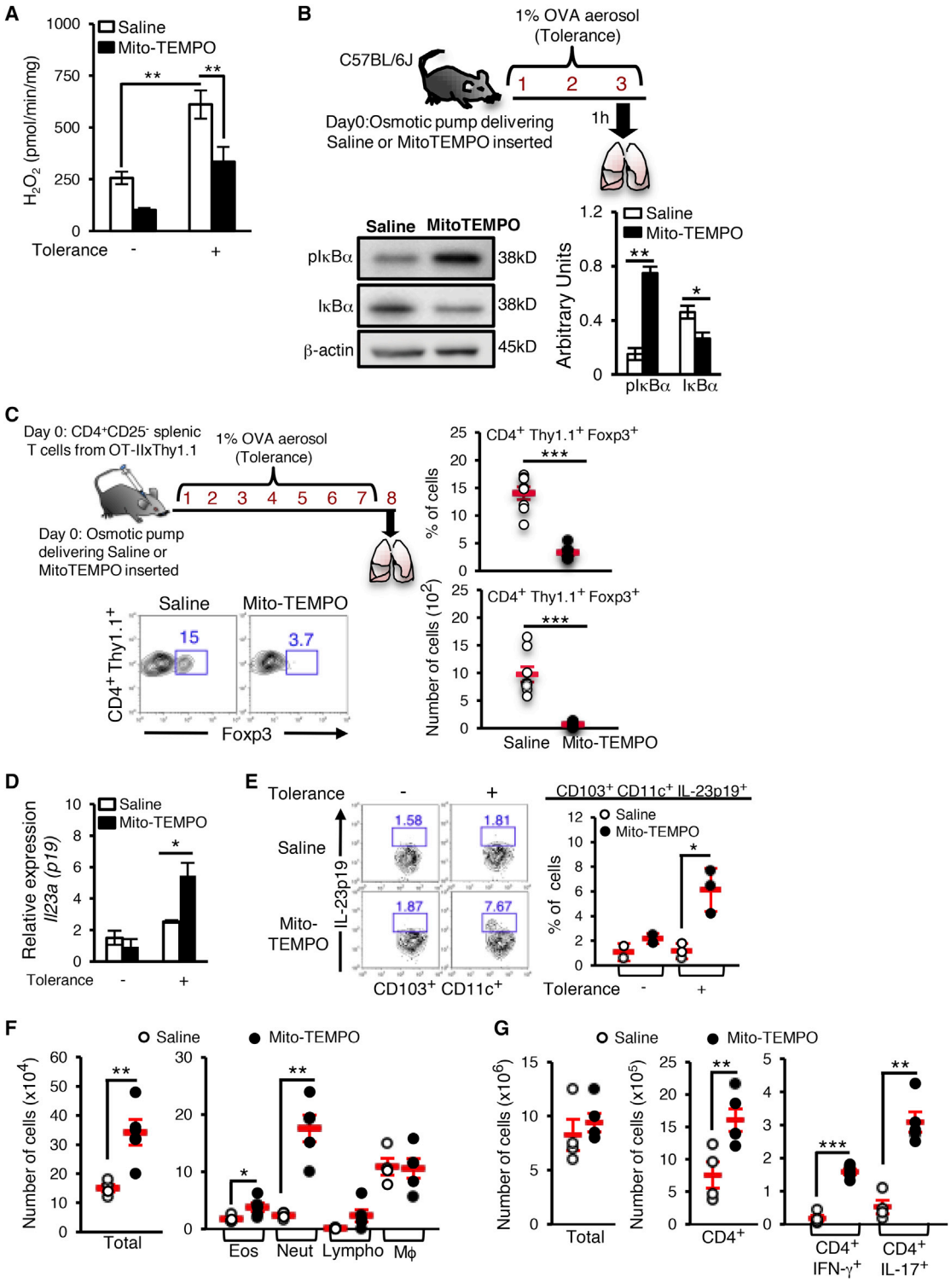

Figure 6. Absence of PPARγ-Dependent Mitochondrial ROS Generation in CD11c$^+$ Cells Induces a T_H1/T_H17 Immune Response

Osmotic pumps delivering either saline or Mito-TEMPO (0.7 mg/kg/day) were surgically inserted in C57/BL6J mice that were then exposed to inhaled OVA (as indicated).

(A) Amplex Red assay was used to quantitate H_2O_2 generation in sorted lung CD11c$^+$ cells. Combined data from two independent experiments are expressed as mean ± SEM.

(B) Representative western blot and densitometry quantification to detect expression of pIκBα and total IκBα levels in lung CD11c$^+$ cells are shown.

(legend continued on next page)

can be exploited (Pascual et al., 2005). Taken together, diverse mechanisms can be utilized by PPARγ to exercise its anti-inflammatory effects, which also may depend on the specific ligand engaged by this nuclear receptor.

In summary, our study demonstrates a protective role of mitochondria in $CD11c^+$ cells as a source of beneficial H_2O_2, the generation of which requires PPARγ. In various capacities, mitochondria are now considered master regulators of danger signaling (Galluzzi et al., 2012). While immune tolerance is desirable to blunt allergic and autoimmune diseases, it is an undesirable outcome in cancer that prevents anti-tumor immune responses. In general, oxidative stress is associated with deleterious consequences including tumorigenesis (Finkel, 2003). High levels of H_2O_2 are associated with many cancers (Lisanti et al., 2011), which, based on the results of the present study, may promote Treg cells that impair anti-cancer immunity. Targeting mitochondria by specific small molecules (Murphy, 1997) to either promote or quench H_2O_2 production may provide therapeutic benefit to blunt inflammatory diseases, like asthma and various autoimmune diseases, or to induce anti-tumor immunity.

EXPERIMENTAL PROCEDURES

Mice

C57BL/6J (00664), *PPARγ*$^{fl/fl}$ (004584), and *CD11c-Cre*$^{+/-}$ (008068) mice were purchased from The Jackson Laboratory and were housed in the Department of Laboratory Animal Resources (DLAR) at the University of Pittsburgh. *PPARγ*$^{fl/fl}$ and *CD11c-Cre*$^{+/-}$ mice were bred to generate mice with deletion of PPARγ in $CD11c^+$ cells (*CD11c-Cre*$^{+/-}$-*PPARγ*$^{fl/fl}$) and littermate controls (*PPARγ*$^{fl/fl}$) (Khare et al., 2015). *CD11c-Cre*$^{+/-}$ mice also were used as controls and were found to be functionally similar to *PPARγ*$^{fl/fl}$ mice (data not shown). OT-IIxThy1.1 transgenic mice, a gift from Dr. Lauren Cohn at Yale University, were bred in the DLAR facility. All mice were housed under pathogen-free conditions and used between 6 and 12 weeks of age. All protocols involving animal experiments were approved by the Institutional Animal Care and Use Committee (IACUC) at the University of Pittsburgh.

Exposure of Mice to Antigens to Induce Tolerance and Assessment of Airway Inflammation

The mice were exposed to aerosolized OVA for 3 consecutive days and lung cells were harvested 1 hr after the last exposure, as shown in Figure 1A. For comparison of tolerance models, mice were tolerized by exposure to OVA for 10 consecutive days, as described before (Ostroukhova et al., 2004). In experiments where mice were exposed to the allergen Derp1 of house dust mites, 20 μl LoTox Natural Derp1 protein (nDerp 1, Indoor Biotechnologies) resuspended in PBS at a concentration of 1 mg/ml was intranasally administered once for 3 consecutive days. For assessing the role of ROS in the induction of tolerance versus pro-inflammatory cytokines, mini-osmotic pumps (Alzet model 2001, 1 μl/hr, 7 days and OR Alzet model 2002, 0.5 μl/hr, 14 days), containing either Mito-TEMPO (0.7 mg/kg/day) or saline, were subcutaneously inserted into WT mice under anesthesia. The mice were then subjected to aerosolized OVA for 20 min each day over a 3-day or a 10-day period (McMenamin et al., 1994; Ostroukhova et al., 2004). To test for induction of tolerance, the tolerized mice were subjected to an inflammation model as previously described by us involving intranasal administration of OVA along with the adjuvant cholera toxin (CT, List Biochemicals) (Khare et al., 2013, 2015; Oriss et al., 2005). Mice were challenged with aerosolized OVA daily for the next 7 days. The degree of airway inflammation and/or resistance to antigen challenge (tolerance) was assessed in mice 24 hr following completion of the protocol(s) outlined in the preceding section, as described previously (Khare et al., 2013; Krishnamoorthy et al., 2012; Oriss et al., 2005).

Cell Isolation and Sorting

The lungs of euthanized mice were perfused with sterile PBS, dissected, and enzymatically digested as described previously (Khare et al., 2013, 2015; Oriss et al., 2005). Lung cells were then physically dissociated on a gentleMACS Dissociator (Miltenyi Biotec) according to the manufacturer's protocol. Single-cell suspensions were obtained by passing the dissociated tissue through a 70-μM cell strainer (BD Falcon). Magnetic separation utilizing anti-CD11c microbeads (Miltenyi Biotec) was used to enrich for $CD11c^+$ cells. The lung $CD11c^+$ cells were sorted into $CD11c^+$ DCs (low auto-fluorescence) to greater than 90% purity using a FACSAria cell sorter (BD Immunocytometry Systems) for DC-T cell co-culture.

Antibodies and Flow Cytometry

Cell-surface markers were analyzed on several cell types using a variety of reagents. Cells were stained in 1× PBS containing 2% (w/v) fetal bovine serum (FBS) with anti-CD4-APC or PE-Cy7 (RM4-5, BD Biosciences); anti-CD11c-APC, PercP-Cy5.5, PE-Cy7 (HL3, BD Biosciences); anti-CD103-PE (M290, BD Biosciences); anti-CD11b-PE-Cy7, PE-CF594 (M1/70, BD Biosciences); anti-CD90.1-PE (OX-7, BD Biosciences); anti-MHCII FITC (NIMR4, Southern Biotech); anti-CD45-PE-Cy7 (30F11, Biolegend); anti-Siglec-F-PE, PE-CF594 (E50-2440, BD Biosciences); and anti-F4/80-Alexa fluor 647, PE (BM8, Invitrogen). Intracellular staining was performed according to the manufacturer's instructions. Intracellular staining with anti-IL-17A-PE (eBio17B7, eBioscience) and anti-IFN-γ-FITC (XMG1.2, BD Biosciences) was assessed in cells stimulated for a total of 6 hr with PMA (50 ng/ml, Sigma) and ionomycin (1 μg/ml, Sigma) in the presence of monensin (BD Biosciences) for the final 3 hr of incubation, according to the manufacturer's instructions (BD Biosciences). For intracellular cytokine staining in DCs, lung cells were cultured ex vivo in the presence of monensin alone for 5 hr and stained with anti-IL-23p19-efluor 660 (fc23cpg, eBioscience), according to the manufacturer's instructions. Stained cells were examined on FACSCalibur and FACSAria flow cytometers (BD Immunocytometry Systems), and the data were analyzed using FlowJo software (Tree Star).

Induction of $Foxp3^+$ $CD4^+$ T Cells In Vivo

Treg-depleted $CD4^+$ T ($CD4^+CD25^-$) cells were isolated from OT-IIxThy1.1 spleens as described before (Khare et al., 2015; Krishnamoorthy et al., 2012), and they were adoptively transferred intravenously (10^6 cells per

(C) 10^6 $CD4^+$ $CD25^-$ splenic T cells from OT-IIxThy1.1 mice were adoptively transferred following osmotic pump implantation. The recipient mice were exposed to inhaled OVA (upper left panel), and Foxp3 induction in the donor T cells in the lungs of the recipient mice was assessed. Representative flow cytometry data from one of two experiments (bottom left) and frequency (top right) and number (bottom right) of $CD4^+$ $Thy1.1^+$ $Foxp3^+$ T cells are shown. Symbols in the graphs represent individual mice (n = 6); horizontal lines show the mean values and error bars denote SEM.
(D) Expression of *Il23a* (*p19*) mRNA in $CD103^+$ $CD11c^+$ lung cells sorted from naive and tolerized saline- or Mito-TEMPO-treated mice, relative to *hprt1*, is shown.
(E) Flow cytometry analysis (left) and frequency (right) of IL-23p19-expressing lung $CD103^+CD11c^+$ cells from naive and tolerized saline- or Mito-TEMPO-treated mice. Symbols in the graphs represent individual mice (n = 3); horizontal lines show the mean values and error bars denote SEM.
(F and G) Following osmotic pump implantation, mice were tolerized to OVA and tested for induction of tolerance as described in the Experimental Procedures. Then 24 hr after the last treatment, various parameters of inflammation were analyzed. (F) Total cell numbers (left); eosinophils and neutrophils (right) in the BAL fluid; and (G) numbers of total lung cells, $CD4^+$ T cells, and IL-$17A^+$ and IFN-γ^+ $CD4^+$ T cells in the lungs of saline- or Mito-TEMPO-treated mice were enumerated. Symbols in the graphs represent individual mice (n = 5); horizontal lines show the mean values and error bars denote SEM (*$p < 0.05$, **$p < 0.01$, and ***$p < 0.001$).

recipient) into *CD11c-Cre*$^{+/-}$-*PPARγ*$^{fl/fl}$ (PPARγ$^{\Delta APC}$) and *PPARγ*$^{fl/fl}$ (WT) mice, respectively. Then 24 hr following the adoptive transfer of cells, the recipient mice were exposed to OVA aerosols for 10 consecutive days and sacrificed 1 day following the last challenge. PBS-perfused lungs were harvested and single-cell suspensions were prepared. In vivo induction of Foxp3 was assessed by staining for donor mouse strain-specific cell-surface marker anti-CD90.1 along with anti-CD4 and anti-Foxp3. CD4$^+$ T cells positive for donor cell-surface marker were selected for analysis of Foxp3 expression.

RNA Isolation and qRT-PCR or Semiquantitative RT-PCR

Sorted lung CD11c$^+$ cells from CD11c-Cre-PPARγ$^{fl/fl}$ and PPARγ$^{fl/fl}$ mice were lysed using RLT plus Buffer (QIAGEN), and RNA was extracted using an RNeasy Plus Micro kit (QIAGEN) according to the manufacturer's instructions. cDNA was synthesized using a High-Capacity cDNA Reverse Transcription Kit (Life Technologies) and was used as a template for qPCR according to the manufacturer's instructions (Life Technologies). Primer and probe sets for assaying individual gene expression were purchased from Life Technologies (Taqman Gene Expression Assays). The qRT-PCR reactions were carried out using the ABI PRISM 7700 Sequence System (Applied Biosystems) at the Genomics Research Core at the University of Pittsburgh. Results were analyzed using the SDS 2.2.2 software. The mRNA expression was calculated using the $2^{-\Delta Ct}$ method with hprt1 as internal reference control.

PPAR Target PCR Array

Lung CD11c$^+$ cells were sorted from naive or tolerized (OVA-exposed) WT and PPARγ$^{\Delta APC}$ mice. CD11c$^+$ cells isolated from naive WT mice were treated with either vehicle or 10 μM RSG in vitro for 4 hr at 37°C. Total RNA was isolated as described above and subjected to cDNA synthesis using RT^2 First Strand Kit (QIAGEN). Gene expression from four biological replicates was analyzed using RT^2 Profiler PCR Array Mouse PPAR Targets (PAMM-149Z, QIAGEN) according to the manufacturer's instructions. Data analysis was carried out using web-based analysis software available on QIAGEN's website. A heatmap was generated using the HeatMapImage module available at http://genepattern.broadinstitute.org.

CFSE Proliferation Assay

Treg-depleted splenic CD4$^+$ T cells from OT-II mice were labeled with CFSE (Vybrant CFDA-SE cell tracer kit, Invitrogen). Briefly, CD4$^+$ CD25$^-$ T cells were labeled with 5 μM CFSE for 10 min at 37°C and co-cultured in the presence of 1 μg/mL OVA-peptide, with CD11c$^+$ DCs sorted from tolerized PPARγ$^{\Delta APC}$ and WT mice that were pre-treated for 1 hr at 37°C with either vehicle or 10 μM BAY11-7082 (EMD Millipore) at a DC:T cell ratio of 1:10. CD4$^+$ T cell proliferation was assessed after 72 hr using flow cytometry. IL-2 level in culture supernatants was assessed by ELISA.

GC-MS Analysis for FFAs

CD11c$^+$ and CD11c$^-$ cells isolated from the lungs of naive and tolerized WT and PPARγ$^{\Delta APC}$ mice were frozen at −80°C under inert condition and sent to Lipid Maps, Lipidomics Core (University of California, San Diego) for assaying concentrations of FFAs using GC-MS (Quehenberger et al., 2011). For the analysis of FFAs, the biological material was supplemented with a cocktail of deuterated internal fatty acid standards and extracted twice with 0.05 N methanolic HCl/isooctane (1:3, v/v), and the combined isooctane layers were evaporated to dryness. The extracted FFAs were derivatized with pentafluorobenzyl bromide, and the fatty acid esters were analyzed by GC-MS on an Agilent 6890N gas chromatograph equipped with an Agilent 5973 mass selective detector (Agilent). Fatty acid quantitation was achieved by the stable isotope dilution method using concentration curves generated from fatty acid quantitative standards using identical conditions. The raw data obtained then were subjected to analysis and the unknowns compared to the standard curves generated and represented as pmol/10^6 cells.

Western Blot Analysis

Total cell lysates and nuclear and cytoplasmic extracts were prepared from sorted and/or treated CD11c$^+$ and CD11c$^-$ cells as described in the text using lysis buffer (Cell Signaling Technology) and nuclear extraction kit (Panomics), respectively. Lysates (15 μg) were separated on 10% SDS-PAGE gels and then transferred onto polyvinylidene fluoride (PVDF) membranes (Millipore). Nonspecific binding was blocked by incubation in blocking buffer (5% nonfat milk in Tris-buffered saline with Tween [TBST]), followed by sequential incubations with the primary antibody and appropriate horseradish peroxidase-conjugated secondary antibody (Thermo Scientific), each diluted in blocking buffer. Immunoreactive protein was detected using enhanced chemiluminescence (ECL) reagents (Thermo Scientific). Antibodies against IκBα (Santa Cruz Biotechnology), phospho-IκBα, NF-κB subunit p65, c-rel, LSD1 (Cell Signaling Technology), phospho IKKα/β, IKKα/β (Cell Signaling Technology), MnSOD (EMD Millipore), Cu-ZnSOD (Enzo Life Sciences), and β-actin (Cell Signaling Technology) were used for western blot analysis. Densitometric analysis was performed using the ImageJ software.

Chromatin Immunoprecipitation Assay

Chromatin immunoprecipitation (ChIP) assays were done according to the manufacturer's protocol (Pierce) with slight modifications. In brief, CD11c$^+$ cells sorted from the lungs of tolerized (3-day or 10-day model) WT and PPARγ$^{\Delta APC}$ mice were fixed with 1% formaldehyde, quenched using 1 M glycine, lysed, and chromatin digested using ChIP grade Micrococcal Nuclease for 15 min at 37°C. Each pull-down was performed using 0.3 × 10^6 cells with anti-PPARγ (Abcam) using Protein A/G beads. Beads were washed with high-salt and lithium chloride-containing buffers. Chelex-100 Resin was added directly to the beads, and the beads were heated to 95°C for 10 min and incubated at 55°C with Proteinase K. Samples were heated again and supernatants collected were used for PCR with the following ChIP primers: IL-6 (−60 bp) (forward 5′-CCCACCCTCCAACAAAGATT-3′ and reverse 5′-TGAG CTACAGACATCCCCAGT-3′), p19 (−153 bp) (forward 5′-GGAACTGAAGCG GCATACCT-3′ and reverse 5′-AAGGTCCCTGCACTGTAAGG-3′), and p19 (−123 bp) (forward 5′-AGGTGATCTAAGAAGGTGGCT-3′ and reverse 5′-TTCGAAGTCTGGTTCCCGTG-3′). The primers and the respective binding sites were designed and validated using Cold Spring Software's NCBI Primer Blast and Match-1.0.

Chymotrypsin- and Trypsin-like Protease Activity

Lung CD11c$^+$ cells were sorted from 3-day tolerized WT and PPARγ$^{\Delta APC}$ mice, and chymotrypsin-like and trypsin-like activities associated with the proteasome complex were measured from 10,000 cells/well using a homogeneous, luminescent Proteasome-Glo Cell-Based Assay (Promega) according to the manufacturer's instructions. The plates were read on Veritas microplate luminometer (Turner Biosystems).

SOD Activity

Extracts from lung CD11c$^+$ cells sorted from tolerized WT and PPARγ$^{\Delta APC}$ mice were prepared and assayed for SOD activity using a colorimetric SOD activity kit (Cayman Chemicals), according to the manufacturer's instructions.

Detection of ROS

Intracellular H_2O_2 level in CD11c$^+$ cells from naive, in the presence or absence of RSG (1 hr at 37°C), tolerized WT and PPARγ$^{\Delta APC}$ mice (1 hr after the last exposure to inhaled allergen) in the presence or absence of Rot, L-NAME, or Ant A (Sigma) and from WT mice treated with either saline or Mito-TEMPO, administered through mini-osmotic pumps (naive and OVA tolerized), was assessed by Amplex Red assay. For intracellular detection of H_2O_2, lung CD11c$^+$ cells isolated from tolerized WT and PPARγ$^{\Delta APC}$ mice were incubated in the presence or absence of 10 μM PF6-AM (Adooq Bioscience) with or without antigen (10 μg/ml OVA or 1 μg/ml nDerp 1) for 40 min at 37°C. After washing to remove OVA and excess PF6-AM, cells were fixed with 4% paraformaldehyde (PFA) at 4°C for 15 min. For positive control, PF6-AM-loaded cells were exposed to 100 μM H_2O_2 for 15 min before fixing with PFA. To ascertain specificity of PF6-AM for H_2O_2, 10 μM catalase was added to cells along with exogenous H_2O_2. Fixed cells were cytospun onto clean glass slides and processed for imaging. Thresholds were initially set for both WT and PPARγ-deficient cells to minimize nonspecific background signal due to autofluorescence. The images were captured using Olympus Fluoview 1000 confocal microscope with a 20× objective, and quantification was performed using Nikon NIS-Elements software based on uniformly set intensity threshold and normalized per nucleus.

Complex I and Complex III Assay Activity

Complex I and complex III assays were performed in $CD11c^+$ cells lysed by three cycles of freeze/thaw as previously described (Shiva et al., 2007). Briefly, complex I activity was measured by spectrophotometrically monitoring the Rot-sensitive oxidation of NADH at 340 nm. Complex III activity was assessed by spectrophotometrically monitoring the reduction of cytochrome *c* (550 nm) in the presence of ubiquinol.

DMNQ Treatment

Lung $CD11c^+$ cells were sorted from tolerized WT and $PPAR\gamma^{\Delta APC}$ mice, and they were treated ex vivo with 200 μM DMNQ (Enzo Life Sciences) for 1 hr at 37°C. Effects on intracellular H_2O_2 and IκB levels were assessed as described above.

Measurement of OCR

OCR of $CD11c^+$ cells isolated from tolerized WT and $PPAR\gamma^{\Delta APC}$ mice was measured at the basal level. One batch of cells in each group was treated with 200 μM Eto and thereafter with 1 μM Oligo, 1.5 μM FCCP, and 0.1 μM Rot plus 1 μM Ant A using the XF-96 Seahorse system. Cells were plated in triplicate. Seahorse assays were performed in unbuffered DMEM supplemented with 2.5 mM glucose and 1 mM glutamine.

mtDNA Estimation Assay

To determine the ratio of mtDNA to nuclear DNA in $CD11c^+$ cells from naive and tolerized WT and $PPAR\gamma^{\Delta APC}$ mice, $2^{-\Delta\Delta Ct}$ was calculated using difference in Ct values of nucleus-encoded h19 gene and mitochondria-encoded nd1 for each individual sample.

Assessment of Mitochondrial Morphology and Volume

Formalin-fixed $CD11c^+$ cells from naive and tolerized (OVA and Derp1) WT and $PPAR\gamma^{\Delta APC}$ mice were stained using anti-Tom20 (SC-11416, Santa Cruz Biotechnology) to label mitochondria. Cells were co-stained with phalloidin-cy3 (to stain F-actin; R415, Life Technologies) and DAPI (to stain nuclei; Southern Biotech). Confocal z stacks were collected using a 60× (1.43 numerical aperture [NA]) optic on a Nikon A1 equipped with GASP detectors and NIS Elements software (Nikon). The confocal datasets were deconvolved using the 3D Landweber capabilities of Nikon Elements and then imported into Imaris software (Bitplane) for surface rendering and calculation of mitochondrial volumes. Mitochondrial fragmentation was assessed using the sphericity parameter (defined as the ratio of the surface area of the given object to the surface area of a sphere with the same volume as the given object).

Statistical Analyses

Student's unpaired two-tailed t test was used for comparisons between two groups. One-way ANOVA with Tukey's post hoc test was used for comparisons among multiple groups, when appropriate. Differences between groups were considered significant when $p < 0.05$. All statistical analyses were performed using Prism 5 software (GraphPad).

SUPPLEMENTAL INFORMATION

Supplemental Information includes six figures and can be found with this article online at http://dx.doi.org/10.1016/j.celrep.2016.04.060.

AUTHOR CONTRIBUTIONS

A.K. designed and performed experiments, analyzed data, and wrote the manuscript. M.R. designed and performed PCR target array, mitochondrial bioenergetics assays, mtDNA estimation, and ELISA and analyzed data. K.C. designed and performed immunoblotting experiments and ChIP assays and analyzed data. S.D. performed confocal microscopy and analyzed data. C.C carried out OCR measurements and analyzed data. C.K.K. performed Amplex Red assays and analyzed data. K.Q. performed confocal microscopy and analyzed data. C.S.C. and S.C.W. assisted with the assessment of mitochondrial morphology. C.M. assisted with experiments involving osmotic pump installations and animal surgeries and analyzed data. A.K. and T.B.O. performed flow sorting. R. Huff performed animal surgeries. R. Hannum analyzed lung histology. P.R. designed experiments and analyzed data. S.S. designed ROS-related experiments and analyzed data. A.R. conceived the study, designed experiments, analyzed data, and wrote the manuscript.

ACKNOWLEDGMENTS

We thank Dr. Oswald Quehenberger at LIPID MAPS, University of California, San Diego, for his expert help and advice in the analysis of FFAs in lung cells and Morgan Jessup for quantitation of H_2O_2 by imaging. This work was supported by NIH grants AI048927 and AI106684 (to A.R.); HL113956 (to A.R. and P.R.); and HL114453, AI100012, and HL122307 (to P.R.).

Received: December 18, 2015
Revised: March 10, 2016
Accepted: April 15, 2016
Published: May 12, 2016

REFERENCES

Basu, S., Rajakaruna, S., Dickinson, B.C., Chang, C.J., and Menko, A.S. (2014). Endogenous hydrogen peroxide production in the epithelium of the developing embryonic lens. Mol. Vis. *20*, 458–467.

Belvisi, M.G., Hele, D.J., and Birrell, M.A. (2006). Peroxisome proliferator-activated receptor gamma agonists as therapy for chronic airway inflammation. Eur. J. Pharmacol. *533*, 101–109.

Béraud, C., Henzel, W.J., and Baeuerle, P.A. (1999). Involvement of regulatory and catalytic subunits of phosphoinositide 3-kinase in NF-kappaB activation. Proc. Natl. Acad. Sci. USA *96*, 429–434.

Brand, M.D. (2010). The sites and topology of mitochondrial superoxide production. Exp. Gerontol. *45*, 466–472.

Buettner, G.R. (2011). Superoxide dismutase in redox biology: the roles of superoxide and hydrogen peroxide. Anticancer. Agents Med. Chem. *11*, 341–346.

Cates, E.C., Fattouh, R., Wattie, J., Inman, M.D., Goncharova, S., Coyle, A.J., Gutierrez-Ramos, J.C., and Jordana, M. (2004). Intranasal exposure of mice to house dust mite elicits allergic airway inflammation via a GM-CSF-mediated mechanism. J. Immunol. *173*, 6384–6392.

Chance, B., Sies, H., and Boveris, A. (1979). Hydroperoxide metabolism in mammalian organs. Physiol. Rev. *59*, 527–605.

Comhair, S.A., Xu, W., Ghosh, S., Thunnissen, F.B., Almasan, A., Calhoun, W.J., Janocha, A.J., Zheng, L., Hazen, S.L., and Erzurum, S.C. (2005). Superoxide dismutase inactivation in pathophysiology of asthmatic airway remodeling and reactivity. Am. J. Pathol. *166*, 663–674.

Curotto de Lafaille, M.A., Kutchukhidze, N., Shen, S., Ding, Y., Yee, H., and Lafaille, J.J. (2008). Adaptive Foxp3+ regulatory T cell-dependent and -independent control of allergic inflammation. Immunity *29*, 114–126.

da Silva, A.F., Mariotti, F.R., Máximo, V., and Campello, S. (2014). Mitochondria dynamism: of shape, transport and cell migration. Cell. Mol. Life Sci. *71*, 2313–2324.

Dickinson, B.C., Peltier, J., Stone, D., Schaffer, D.V., and Chang, C.J. (2011). Nox2 redox signaling maintains essential cell populations in the brain. Nat. Chem. Biol. *7*, 106–112.

Dikalova, A.E., Bikineyeva, A.T., Budzyn, K., Nazarewicz, R.R., McCann, L., Lewis, W., Harrison, D.G., and Dikalov, S.I. (2010). Therapeutic targeting of mitochondrial superoxide in hypertension. Circ. Res. *107*, 106–116.

Ding, G., Fu, M., Qin, Q., Lewis, W., Kim, H.W., Fukai, T., Bacanamwo, M., Chen, Y.E., Schneider, M.D., Mangelsdorf, D.J., et al. (2007). Cardiac peroxisome proliferator-activated receptor gamma is essential in protecting cardiomyocytes from oxidative damage. Cardiovasc. Res. *76*, 269–279.

Finkel, T. (2003). Oxidant signals and oxidative stress. Curr. Opin. Cell Biol. *15*, 247–254.

Forman, H.J., and Kennedy, J.A. (1974). Role of superoxide radical in mitochondrial dehydrogenase reactions. Biochem. Biophys. Res. Commun. *60*, 1044–1050.

Furuhashi, M., and Hotamisligil, G.S. (2008). Fatty acid-binding proteins: role in metabolic diseases and potential as drug targets. Nat. Rev. Drug Discov. *7*, 489–503.

Galluzzi, L., Kepp, O., and Kroemer, G. (2012). Mitochondria: master regulators of danger signalling. Nat. Rev. Mol. Cell Biol. *13*, 780–788.

Guillou, H., Zadravec, D., Martin, P.G., and Jacobsson, A. (2010). The key roles of elongases and desaturases in mammalian fatty acid metabolism: Insights from transgenic mice. Prog. Lipid Res. *49*, 186–199.

Guth, A.M., Janssen, W.J., Bosio, C.M., Crouch, E.C., Henson, P.M., and Dow, S.W. (2009). Lung environment determines unique phenotype of alveolar macrophages. Am. J. Physiol. Lung Cell. Mol. Physiol. *296*, L936–L946.

Hayden, M.S., and Ghosh, S. (2008). Shared principles in NF-kappaB signaling. Cell *132*, 344–362.

James, A.M., Collins, Y., Logan, A., and Murphy, M.P. (2012). Mitochondrial oxidative stress and the metabolic syndrome. Trends Endocrinol. Metab. *23*, 429–434.

Kalyanaraman, B., Darley-Usmar, V., Davies, K.J., Dennery, P.A., Forman, H.J., Grisham, M.B., Mann, G.E., Moore, K., Roberts, L.J., 2nd, and Ischiropoulos, H. (2012). Measuring reactive oxygen and nitrogen species with fluorescent probes: challenges and limitations. Free Radic. Biol. Med. *52*, 1–6.

Karin, M., and Ben-Neriah, Y. (2000). Phosphorylation meets ubiquitination: the control of NF-[kappa]B activity. Annu. Rev. Immunol. *18*, 621–663.

Katano-Toki, A., Satoh, T., Tomaru, T., Yoshino, S., Ishizuka, T., Ishii, S., Ozawa, A., Shibusawa, N., Tsuchiya, T., Saito, T., et al. (2013). THRAP3 interacts with HELZ2 and plays a novel role in adipocyte differentiation. Mol. Endocrinol. *27*, 769–780.

Khare, A., Krishnamoorthy, N., Oriss, T.B., Fei, M., Ray, P., and Ray, A. (2013). Cutting edge: inhaled antigen upregulates retinaldehyde dehydrogenase in lung CD103+ but not plasmacytoid dendritic cells to induce Foxp3 de novo in CD4+ T cells and promote airway tolerance. J. Immunol. *191*, 25–29.

Khare, A., Chakraborty, K., Raundhal, M., Ray, P., and Ray, A. (2015). Cutting Edge: Dual Function of PPARγ in CD11c+ Cells Ensures Immune Tolerance in the Airways. J. Immunol. *195*, 431–435.

Korn, S.H., Wouters, E.F., Vos, N., and Janssen-Heininger, Y.M. (2001). Cytokine-induced activation of nuclear factor-kappa B is inhibited by hydrogen peroxide through oxidative inactivation of IkappaB kinase. J. Biol. Chem. *276*, 35693–35700.

Krishnamoorthy, N., Khare, A., Oriss, T.B., Raundhal, M., Morse, C., Yarlagadda, M., Wenzel, S.E., Moore, M.L., Peebles, R.S., Jr., Ray, A., and Ray, P. (2012). Early infection with respiratory syncytial virus impairs regulatory T cell function and increases susceptibility to allergic asthma. Nat. Med. *18*, 1525–1530.

Lambrecht, B.N., and Hammad, H. (2012). Lung dendritic cells in respiratory viral infection and asthma: from protection to immunopathology. Annu. Rev. Immunol. *30*, 243–270.

Lin, V.S., Dickinson, B.C., and Chang, C.J. (2013). Boronate-based fluorescent probes: imaging hydrogen peroxide in living systems. Methods Enzymol. *526*, 19–43.

Lisanti, M.P., Martinez-Outschoorn, U.E., Lin, Z., Pavlides, S., Whitaker-Menezes, D., Pestell, R.G., Howell, A., and Sotgia, F. (2011). Hydrogen peroxide fuels aging, inflammation, cancer metabolism and metastasis: the seed and soil also needs "fertilizer". Cell Cycle *10*, 2440–2449.

Lombardi, A., Grasso, P., Moreno, M., de Lange, P., Silvestri, E., Lanni, A., and Goglia, F. (2008). Interrelated influence of superoxides and free fatty acids over mitochondrial uncoupling in skeletal muscle. Biochim. Biophys. Acta *1777*, 826–833.

Loschen, G., Azzi, A., Richter, C., and Flohé, L. (1974). Superoxide radicals as precursors of mitochondrial hydrogen peroxide. FEBS Lett. *42*, 68–72.

McMenamin, C., Pimm, C., McKersey, M., and Holt, P.G. (1994). Regulation of IgE responses to inhaled antigen in mice by antigen-specific gamma delta T cells. Science *265*, 1869–1871.

Murphy, M.P. (1997). Selective targeting of bioactive compounds to mitochondria. Trends Biotechnol. *15*, 326–330.

Murphy, M.P. (2009). How mitochondria produce reactive oxygen species. Biochem. J. *417*, 1–13.

Nethery, D., Callahan, L.A., Stofan, D., Mattera, R., DiMarco, A., and Supinski, G. (2000). PLA(2) dependence of diaphragm mitochondrial formation of reactive oxygen species. J. Appl. Physiol. *89*, 72–80.

Odegaard, J.I., Ricardo-Gonzalez, R.R., Goforth, M.H., Morel, C.R., Subramanian, V., Mukundan, L., Red Eagle, A., Vats, D., Brombacher, F., Ferrante, A.W., and Chawla, A. (2007). Macrophage-specific PPARgamma controls alternative activation and improves insulin resistance. Nature *447*, 1116–1120.

Oliveira-Marques, V., Marinho, H.S., Cyrne, L., and Antunes, F. (2009). Role of hydrogen peroxide in NF-kappaB activation: from inducer to modulator. Antioxid. Redox Signal. *11*, 2223–2243.

Oriss, T.B., Ostroukhova, M., Seguin-Devaux, C., Dixon-McCarthy, B., Stolz, D.B., Watkins, S.C., Pillemer, B., Ray, P., and Ray, A. (2005). Dynamics of dendritic cell phenotype and interactions with CD4+ T cells in airway inflammation and tolerance. J. Immunol. *174*, 854–863.

Ostroukhova, M., Seguin-Devaux, C., Oriss, T.B., Dixon-McCarthy, B., Yang, L., Ameredes, B.T., Corcoran, T.E., and Ray, A. (2004). Tolerance induced by inhaled antigen involves CD4(+) T cells expressing membrane-bound TGF-beta and FOXP3. J. Clin. Invest. *114*, 28–38.

Parry, J.D., Pointon, A.V., Lutz, U., Teichert, F., Charlwood, J.K., Chan, P.H., Athersuch, T.J., Taylor, E.L., Singh, R., Luo, J., et al. (2009). Pivotal role for two electron reduction in 2,3-dimethoxy-1,4-naphthoquinone and 2-methyl-1,4-naphthoquinone metabolism and kinetics in vivo that prevents liver redox stress. Chem. Res. Toxicol. *22*, 717–725.

Pascual, G., Fong, A.L., Ogawa, S., Gamliel, A., Li, A.C., Perissi, V., Rose, D.W., Willson, T.M., Rosenfeld, M.G., and Glass, C.K. (2005). A SUMOylation-dependent pathway mediates transrepression of inflammatory response genes by PPAR-gamma. Nature *437*, 759–763.

Pasparakis, M. (2009). Regulation of tissue homeostasis by NF-kappaB signalling: implications for inflammatory diseases. Nat. Rev. Immunol. *9*, 778–788.

Poole, D.C., Sexton, W.L., Farkas, G.A., Powers, S.K., and Reid, M.B. (1997). Diaphragm structure and function in health and disease. Med. Sci. Sports Exerc. *29*, 738–754.

Quehenberger, O., Armando, A.M., and Dennis, E.A. (2011). High sensitivity quantitative lipidomics analysis of fatty acids in biological samples by gas chromatography-mass spectrometry. Biochim. Biophys. Acta *1811*, 648–656.

Schneider, C., Nobs, S.P., Kurrer, M., Rehrauer, H., Thiele, C., and Kopf, M. (2014). Induction of the nuclear receptor PPAR-γ by the cytokine GM-CSF is critical for the differentiation of fetal monocytes into alveolar macrophages. Nat. Immunol. *15*, 1026–1037.

Sena, L.A., Li, S., Jairaman, A., Prakriya, M., Ezponda, T., Hildeman, D.A., Wang, C.R., Schumacker, P.T., Licht, J.D., Perlman, H., et al. (2013). Mitochondria are required for antigen-specific T cell activation through reactive oxygen species signaling. Immunity *38*, 225–236.

Shiva, S., Sack, M.N., Greer, J.J., Duranski, M., Ringwood, L.A., Burwell, L., Wang, X., MacArthur, P.H., Shoja, A., Raghavachari, N., et al. (2007). Nitrite augments tolerance to ischemia/reperfusion injury via the modulation of mitochondrial electron transfer. J. Exp. Med. *204*, 2089–2102.

Steinman, R.M. (2012). Decisions about dendritic cells: past, present, and future. Annu. Rev. Immunol. *30*, 1–22.

Stríz, I., Wang, Y.M., Svarcová, I., Trnka, L., Sorg, C., and Costabel, U. (1993). The phenotype of alveolar macrophages and its correlation with immune cells in bronchoalveolar lavage. Eur. Respir. J. *6*, 1287–1294.

Tschopp, J. (2011). Mitochondria: Sovereign of inflammation? Eur. J. Immunol. *41*, 1196–1202.

Wahli, W., and Michalik, L. (2012). PPARs at the crossroads of lipid signaling and inflammation. Trends Endocrinol. Metab. *23*, 351–363.

Wakil, S.J., and Abu-Elheiga, L.A. (2009). Fatty acid metabolism: target for metabolic syndrome. J. Lipid Res. *50* (*Suppl*), S138–S143.

Wolf, H.P., and Brenner, K.V. (1988). The effect of etomoxir on glucose turnover and recycling with [1-14C], [3-3H]-glucose tracer in pigs. Horm. Metab. Res. *20*, 204–207.

Xia, Y., Dawson, V.L., Dawson, T.M., Snyder, S.H., and Zweier, J.L. (1996). Nitric oxide synthase generates superoxide and nitric oxide in arginine-depleted cells leading to peroxynitrite-mediated cellular injury. Proc. Natl. Acad. Sci. USA *93*, 6770–6774.

Yoo, H.Y., Chang, M.S., and Rho, H.M. (1999). Induction of the rat Cu/Zn superoxide dismutase gene through the peroxisome proliferator-responsive element by arachidonic acid. Gene *234*, 87–91.